Comparison of rotating cylinder and loop methods for testing CO_2 corrosion inhibitors

S. NESIC
G. T. SOLVI
S. SKJERVE

A study was carried out to investigate the effect of various hydrodynamic parameters on the corrosion rate of low carbon steel in CO_2 environments in the presence of inhibitors. Two different flow geometries, rotating cylinder and pipe flow, were studied simultaneously in the same electrolyte within a glass loop. Comparisons were also carried out at room temperature, pH 4–6, partial pressure of CO_2 1 bar, and velocity 0–13 m s^{-1}. The hydrodynamic conditions studied cover the range from stagnant to highly turbulent flow. The corrosion process was monitored using polarisation resistance, potentiodynamic sweep, and electrochemical impedance. Comparison of the two flow geometries was carried out in terms of the hydrodynamics, mass transfer rates, CO_2 corrosion rates, and corrosion mechanisms. The measured mass transfer rates were found to agree well with previously published correlations for the rotating cylinder and straight pipe flow. In the case of CO_2 corrosion without inhibitors, it was possible to achieve good agreement between corrosion rates in the two flow geometries by ensuring the same water chemistry and mass transfer conditions. This conclusion is valid for the case when no protective corrosion product or scale is present. With inhibitors present, the performance of both amine and imidazoline based inhibitors measured using the rotating cylinder was identical to that in the straight pipe flow geometry. The performance of the inhibitors was not significantly affected by flowrate in the range 2–10 m s^{-1} (corresponding to shear stresses of 13 and 222 Pa respectively).

At the time the work was carried out, Dr Nesic and Mr Solvi were at the Institute for Energy Technology, Instituttveien 18, PO Box 40, N–2007 Kjeller, Norway and Ms Skjerve was with Statoil, 70004 Trondheim, Norway. Dr Nesic is now in the Department of Mechanical Engineering, University of Queensland, Brisbane, Qld 4072, Australia. *Manuscript received 20 November 1995; in final form 15 January 1997.*

LIST OF SYMBOLS

A	area, m^2
B	polarisation resistance constant, V
d_p, d_c	pipe and cylinder diameter, m
D	diffusion coefficient, $m^2\ s^{-1}$
f	Fanning friction factor ($=2\tau/\rho v^2$)
F	Faraday constant, 96 490 C mol^{-1}
i	current density, A m^{-2}
i^d_{lim}	diffusion limiting current density, A m^{-2}
k_m	mass transfer coefficient, m s^{-1}
l	characteristic length, m
L	pipe length, m
p	pressure, bar
p_{CO_2}	partial pressure of CO_2 gas, bar
Q	volumetric flow rate, $m^3\ s^{-1}$
Re	Reynolds number $= \rho v l/\mu$
Sc	Schmidt number $= \mu/\rho D$
Sh	Sherwood number $= k_m l/D$
T	temperature, °C
v	velocity, m s^{-1}
ε	pipe roughness, m
η	overpotential, V
μ	viscosity, kg $m^{-1}\ s^{-1}$
ρ	density, kg m^{-3}
τ_w	wall shear stress, Pa
ω	rotation (angular) speed, rad s^{-1}

Subscripts

p	pipe
c	cylinder

INTRODUCTION

Corrosion can be affected by flow in various ways depending on the mechanism governing the corrosion process. Two major cases can be arbitrarily distinguished: first, the effect of flow on corrosion when surface films are not present and, second, the effect of flow on corrosion in the presence of surface films (corrosion products, scales, inhibitors, etc.). In the first, the 'no film' case, the primary effect of flow on corrosion is through the mass transfer of the species involved in the corrosion reaction at the metal surface. When surface films are present, they can reduce the corrosion rate by hindering the transport of species involved in the electrochemical reactions at the metal surface. In the case of inhibitor films, parts of the surface are 'blocked' by the inhibitor and the electrochemical double layer can be altered. It is often argued that inhibitor films can be locally or globally removed by the flow, leading to very high corrosion rates. It is not yet clear which forces are responsible for film removal. In the literature, the onset of film removal has been associated with the average wall 'shear stress'[1] and near wall 'turbulence fluctuations'[2] or 'turbulent bursts'.[3] However, there has been no clear and detailed study in which this was investigated. The present study was aimed at establishing the effect of flow on CO_2 corrosion with and without protective inhibitor films.

EXPERIMENTAL

Glass loop

The experimental glass flow loop used in the present study is shown in Fig. 1. The loop was built to handle two phase oil–water flow. However, only the single phase water flow experiments are presented here. Glass was selected as the main loop material for two reasons: it enables application of aggressive cleaning procedures (in between experiments with inhibitors) and it is optically transparent (important, especially in two phase flow experiments).

Two test sections were mounted in the loop: the straight pipe (SP) and the rotating cylinder (RC). The same electrolyte was circulated through both test sections guaranteeing identical water chemistry conditions for the

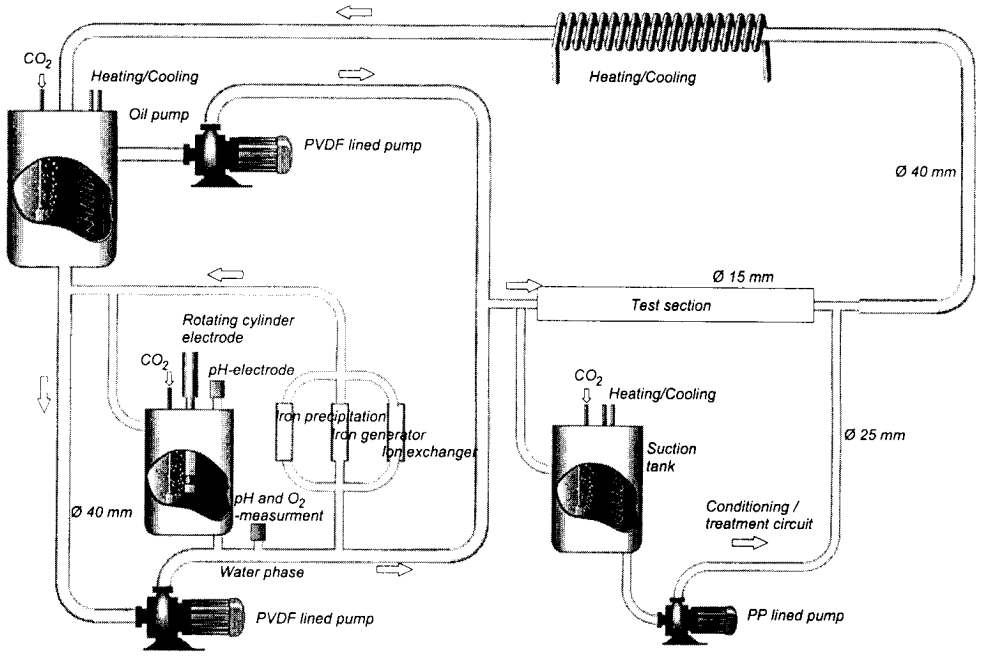

1 *Schematic diagram of glass flow loop*

corrosion process. The same idea was previously used by Efird *et al.*[4] in a similar study. An enlarged view of the SP test section made from polytetrafluoroethylene (PTFE) is shown in Fig. 2. Two or three steel specimens were flush mounted in the pipe ($d_p = 15$ mm). Optionally, up to three additional pipe test sections can be added to the existing one, in series. The RC ($d_c = 10$ mm) mounted in a cylinder glass chamber with all the measuring equipment is shown in Fig. 3.

Most components of the loop, including the valves, were made from borosilicate glass and PTFE. Some minor components (mostly fittings) were made from polypropylene (PP), polyvinyl chloride (PVC), polyvinyl difluoride (PVDF), fluoroelastomer, AISI 316 stainless steel, titanium grade 2, and Hastelloy C-276 alloy. The construction of the loop enabled reliable control of the flow parameters, water chemistry, and temperature as well as stable and reliable automatic operation of the loop for extended periods of time (up to several weeks).

Water chemistry

Water chemistry is one of the most important factors affecting the corrosion rate, so significant attention has been given to this matter. Water preparation included: water purification by distillation or reverse osmosis and bubbling with CO_2, typically for one day, before the experiment. Continuous CO_2 bubbling was maintained throughout the experiment. The O_2 content was measured occasionally and kept below 50 ppb throughout the experiment. Additions of HCl and $NaHCO_3$ were used to achieve the desired pH. It was possible to control the Fe^{2+} concentration by use of an iron generator (for increasing Fe^{2+} concentration), an ion exchanger (which can substitute the Fe^{2+} in the solution by H^+ or Na^+ ions), and a high temperature iron precipitator. When needed, samples of the loop water were taken for analysis to determine the amount of dissolved CO_2 and the concentration of Fe^{2+}. The pH was measured with two independent electrodes to register a possible drift: one was placed in a sidestream

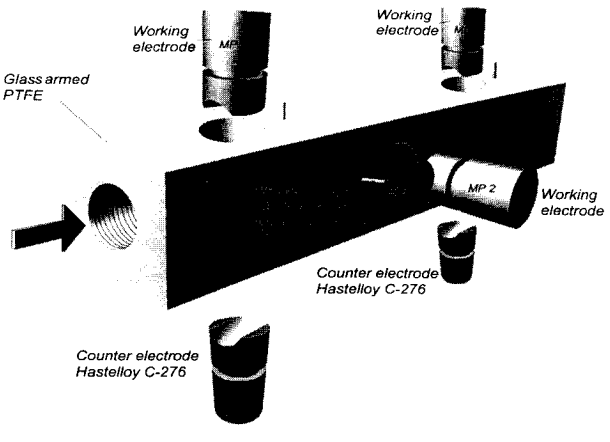

2 *Schematic diagram of straight pipe section made from PTFE*

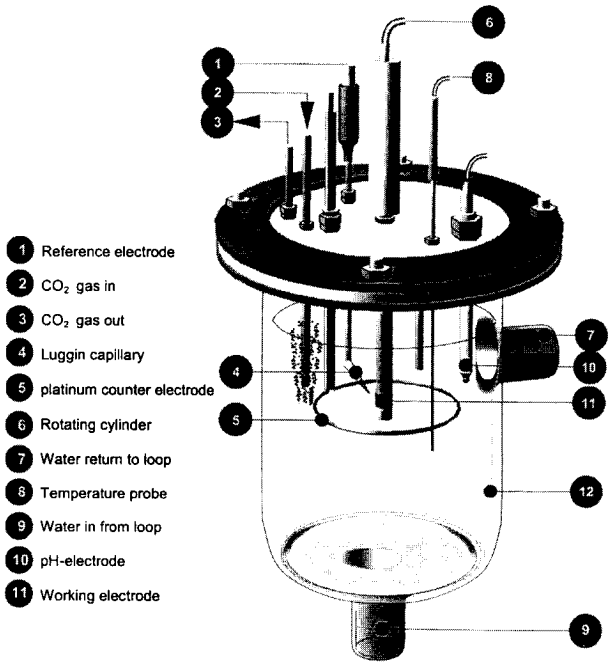

3 *Schematic diagram of rotating cylinder test section made from glass*

taken from the main circuit and the other was placed in the RC chamber. The water temperature was kept constant at the desired temperature ± 1 K.

Material

In all experiments, a low carbon X65 steel was tested. This is a typical pipeline steel, the chemical composition of which is Fe–0·064C–0·25Si–1·54Mn–0·013P–0·001S–0·05Cr–0·07Mo–0·04Ni–0·041Al–0·04Cu–0·041Nb–0·002Sn–0·002Ti–0·035V (wt-%).

Inhibitor composition

Both inhibitors studied were commercial formulations as delivered by the supplier. Very little information was available on the composition of the inhibitor packages.

According to the supplier, the amine based inhibitor (ABI) is composed of 30–60% amine based fatty acid derivatives, the rest being water. An antioxidant is also present which helps in preparation of the metal surface for adsorption. The supplier characterises the ABI as a single component filming corrosion inhibitor (no surfactants present). It is believed that the amine molecules are chemically bound to the metal surface.

Less was known about the composition of the imidazoline based inhibitor (IBI). According to the supplier, the IBI is composed of 10–30% imidazoline salts and 10–30% butylglycol, the rest probably being water. It is believed that imidazoline molecules are chemically bound to the metal surface and offer corrosion protection. It is likely that the butylglycol is added as a solvent.

Corrosion measurements

The corrosion process was studied using the electrochemical techniques: polarisation resistance, electrochemical impedance, and potentiodynamic sweep. The accuracy of the polarisation resistance measurements for determining the corrosion rate was checked occasionally against weight loss. By using a B value of 20 mV as a first approximation, agreement within 10% was found. A three electrode setup was used in all electrochemical experiments both in the SP and the RC test sections. In the SP test section (Fig. 2), the working and the counter electrodes were mounted flush with the pipe wall so that minimal flow disturbance was created. The working electrode made from carbon steel and the counter electrode made from Hastelloy C–276 were identical in shape (area 2·9 cm^2), and were mounted diametrically opposite each other so that a 'uniform' current distribution was obtained during polarisation experiments. An external Ag/AgCl reference electrode (filled with saturated KCl) was connected to the cell via an ion conducting porous wooden plug.

In the RC test section (Fig. 3), a carbon steel working electrode was mounted on a rotator with a speed control unit (0–5000 rev min^{-1}). The specimen was machined from the parent material into a cylinder 10 mm in diameter and 10 mm in length. The exposed area of the specimen was 3·14 cm^2. A concentric platinum wire ring served as a counter electrode. An external Ag/AgCl reference electrode was connected to the cell via a Luggin capillary with a porous wooden plug. The rotating speed of the working electrode was occasionally controlled with a stroboscope. Electrochemical measurements were made with a Gamry Instruments potentiostat with an eight channel multiplexer connected to a PC 486/25 computer.

Procedure

The glass loop was filled with ~ 56 L of electrolyte: distilled water + 1 wt-%NaCl. The CO_2 was then continuously bubbled through the electrolyte (usually for 24 h before the experiment) to deoxygenate and saturate the solution with CO_2. Monitoring of pH and O_2 concentration was used to judge when the solution reached equilibrium with the bubbling CO_2 gas. Then, the pH was adjusted by adding HCl or $NaHCO_3$. Before immersion, the carbon steel specimen surfaces were polished with 500 and 1000 grit SiC paper, degreased with acetone, and washed with alcohol. After preparation, the specimens were inserted into the loop. Subsequently, polarisation resistance measurements were started. In the inhibitor experiments, the specimens corroded in the loop for some time at $v_p = v_c = 2$ m s^{-1} (3820 rev min^{-1}) before the introduction of the inhibitor (3 h for ABI and 19 h for IBI). The polarisation resistance measurements were conducted by polarising the working electrode ± 5 mV from the free corrosion potential and scanning at 0·2 mV s^{-1}. The solution resistance was measured independently using electrochemical impedance and subtracted from the polarisation resistance. The electrochemical impedance measurements were conducted by applying a sinusoidal oscillating potential to the working electrode, ± 5 mV_{rms} around the free corrosion potential using the frequency range 10 mHz–100 kHz. At the end of each experiment, the potentiodynamic sweeps were conducted, starting 300–600 mV below and finishing 150–200 mV above the free corrosion potential. The typical scanning rate used was 0·2 mV s^{-1}.

Difficulties

Numerous difficulties were encountered during the experimental programme. This experience might be instructive for other researchers in the area. It was found that even very small quantities of contamination leaking from loop components could be detrimental and lead to erroneous measurements. During the experiments, contamination occurred as a result of lead dissolving from a minute seal in a rotameter used to monitor the flowrate through a bypass stream. It was also found that tin was dissolving from a graphite pump bearing. In both cases, the contaminating metals were deposited on the surface of the specimen. The most serious contamination was discovered to come from a short nitrile rubber hose used to connect the pumps with the loop. The mysterious contaminant was a very effective corrosion inhibitor in itself. When the experiments with inhibitors were started, another problem appeared. It seemed as if there was an additional contaminant in the loop which did not affect the baseline corrosion rate but affected the performance of the inhibitor. In other words, the inhibitor was 'inhibited'. The source of this contamination in the loop was particularly difficult to discover. After an in depth investigation, it was discovered by scanning electron microscopy (SEM) and X-ray analysis that the source of the problem was a very thin layer of molybdenum present on the surface of the specimen which prevented the inhibitor from adsorbing. The source of the molybdenum was a few minor components of the loop (fittings and small tubes) made from stainless AISI 316 steel. During the washing of the loop between experiments, when HCl solution was used, the protective passive layer on the AISI 316 steel was destroyed and molybdenum began dissolving. All of the above mentioned sources of contamination had to be removed before meaningful measurements could be made.

RESULTS AND DISCUSSION

Selection of an adequate laboratory scale apparatus for testing of flow effects in CO_2 corrosion is a difficult task. The selected experimental setup must have well defined hydrodynamic and mass transfer characteristics. In addition, good control of water chemistry must be possible. The straight pipe and rotating cylinder test sections used in the present experiments satisfy both of the above requirements. By testing the two flow geometries using the

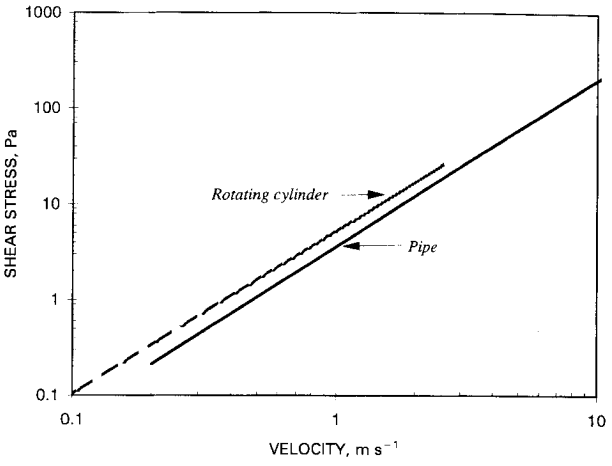

4 *Calculated shear stress as function of velocity at* $T = 20°C$, $d_c = 0{\cdot}01$ *m*, $d_p = 0{\cdot}015$ *m*

same electrolyte, it could be assumed that the water chemistries were identical. This enabled the differences in the CO_2 corrosion process that arise from hydrodynamic and mass transfer considerations to be studied.

Fluid flow

From a practical point of view, the primary interest is in turbulent flow regimes. For pipe flow, at Reynolds numbers below $Re_p = \rho v_p d_p/\mu = 2000$, laminar flow is encountered. For $2000 < Re_p < 3000$, a transition to turbulent flow occurs. Translated to the present experimental conditions ($d_p = 15$ mm, $T = 20°C$), turbulent flow was achieved for all velocities greater than 0·2 m s^{-1}. At higher temperatures, the transition occurs at even lower velocities. For a RC geometry, laminar flow is typically encountered for Reynolds numbers $Re_c = \rho v_c d_c/\mu < 200$ (where $v_c = \omega d_c/2$ is the peripheral velocity of the RC). This means that under the present conditions ($d_c = 10$ mm, $T = 20°C$), turbulent flow was encountered in the vicinity of the cylinder for rotational speeds above $\omega = 40$ rev min^{-1}. This corresponds to a RC peripheral velocity of $v_2 = 0{\cdot}02$ m s^{-1}.

The shear stress exerted at the wall in pipe flow can be determined from the pressure gradient along a pipe

$$\tau_w = (\Delta p/\Delta L)(d_p/4) \quad . . . . . (1)$$

However, the pressure drop in the experiments was not measured, so the shear stress had to be determined from existing correlations. For turbulent pipe flow, such a relationship can be found only empirically in terms of the laws of friction. One such well known correlation for high Reynolds numbers ($Re_p > 10^5$) is the Coolebrook equation[6]

$$\frac{1}{f_p^{1/2}} = -4\log\left(\frac{\varepsilon}{3{\cdot}7 d_p} + \frac{1{\cdot}256}{Re_p f_p^{1/2}}\right) \quad . . . . . (2)$$

which is valid when $Re_p > 3000$. For the rotating cylinder in the case of a turbulent flow regime (smooth surfaces), the friction factor is[6]

$$f_c = 0{\cdot}158\, Re_c^{-0{\cdot}3} \quad . . . . . (3)$$

for $Re_c > 300$. In Fig. 4, the calculated shear stress is compared for SP and RC flows in the loop at 20°C. The velocity plotted on the x axis is the average cross-sectional velocity ($v_p = Q_p/A_p$) for SP flow and peripheral velocity ($v_c = \omega d_c/2$) for RC flow. The smooth surface correlations were used to calculate the shear stress. This is justifiable as, in the present experiments, the surface roughness varied from $\varepsilon/d_p \sim 1 \times 10^{-4}$ for the freshly polished specimens to $\varepsilon/d_p \sim 4 \times 10^{-4}$ for heavily corroded surfaces (determined by looking at the surface cross-section using SEM). Calculated using the above correlations, even for the highest velocities, the effect of maximum roughness changed shear stress by less than 10%.

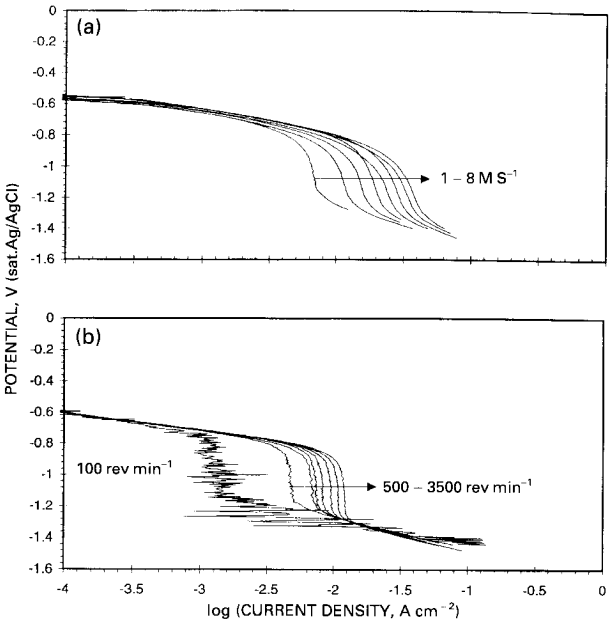

a pipe flow; *b* rotating cylinder

5 *Potentiodynamic sweep: effect of velocity on mass transfer limiting currents; pH 3,* $T = 20°C$, $p_{N_2} = p_{total} = 1$ *bar,* $d_c = 0{\cdot}01$ *m,* $d_p = 0{\cdot}015$ *m*

From Fig. 4, it can be seen that, with the RC, shear stresses up to 25 Pa could be achieved at maximum rotation speed (5000 rev min^{-1}, which corresponds to $v_2 = 2{\cdot}61$ m s^{-1}). In the SP, as much as 300 Pa was achieved at $v_p = 12$ m s^{-1}. For the 'equivalent' velocity ($v_p = v_c$), similar shear stresses were obtained for the two flow geometries. This is true only when the RC and SP diameters are of the same order of magnitude, which was the case in the present loop. Most of the experiments were carried out at $v_p = v_c = 2$ m s^{-1} (3820 rev min^{-1}), for which the calculated shear stresses were 16 and 12 Pa in the RC and SP respectively.

Mass transfer

According to general understanding of the CO_2 corrosion mechanisms, mass transfer is important primarily at pH < 5 when it affects the limiting currents for H^+ reduction. As this pH range is in the present domain of interest, mass transfer characterisation of the two flow geometries in the loop was carried out. This was achieved by conducting experiments at pH 3 in a 1%NaCl aqueous solution purged with N_2 gas. Under these conditions, the dominant cathodic reaction for modest overpotentials ($\eta < -0{\cdot}5$ V) is the reduction of H^+ ions. For overpotentials of $-0{\cdot}2 < \eta < -0{\cdot}5$ V, it was possible to obtain clear mass transfer limiting currents, as shown in Fig. 5. Potentiodynamic sweeps were conducted beginning from the corrosion potential and finishing 0·8 V below. This was repeated for various SP velocities and RC speeds. The measured limiting currents were converted to the mass transfer coefficient by using

$$k_m = i^d_{lim(H^+)}/F10^{-pH} \quad . . . . . (4)$$

Correlations for mass transfer coefficients for turbulent flow are well established in the literature for the two flow geometries under investigation. In the case of straight pipe flow, the correlation of Berger and Hau[7] can be used

$$Sh_p = k_m d_p/D = 0{\cdot}0165 Re_p^{0{\cdot}86} Sc^{0{\cdot}33} \quad . . . . . (5)$$

For the rotating cylinder flow, the correlation of Eisenberg *et al.*[8] is appropriate

$$Sh_c = k_m d_c/D = 0{\cdot}0791 Re_c^{0{\cdot}7} Sc^{0{\cdot}356} \quad . . . . . (6)$$

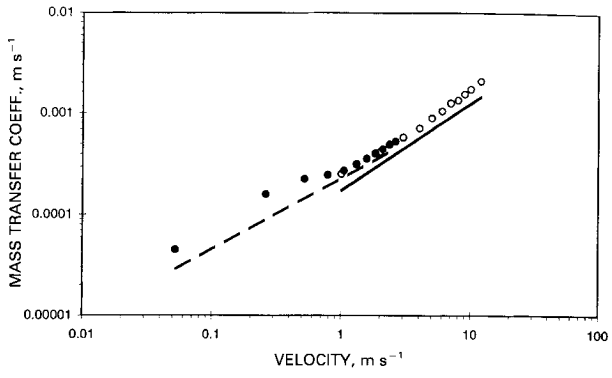

○ measured, pipe flow; ● measured, rotating cylinder; — Ref. 7 correlation; -- Ref. 8 correlation

6 *Measured and predicted mass transfer coefficients as function of velocity for two flow geometries: pH 3, $T = 20°C$, $p_{N_2} = p_{total} = 1$ bar, $d_c = 0{\cdot}01$ m, $d_p = 0{\cdot}015$ m*

The measured and calculated mass transfer coefficients as a function of velocity are shown in Fig. 6. The value $D_{(H^+)} = 9{\cdot}31 + 10^{-9}\ m^2\ s^{-1}$ was used to obtain the value of k_m from the Sherwood number.[9] In Fig. 6, it has again been arbitrarily decided to compare the k_m values for the 'equivalent' velocity ($v_p = v_c$). However, the most important conclusion is that, for both the RC and the SP flows, the agreement between the measured mass transfer coefficient in the experimental loop and that predicted using the above correlations is good. This means that good control of the mass transfer conditions was achieved in the loop for both flow geometries. For higher velocities, a somewhat larger discrepancy between predicted and measured k_m was obtained for the SP flow. It can be assumed that the working electrodes in the SP test section (Fig. 2), which were only 20 mm in length ($1{\cdot}33d_p$), were too short to completely eliminate the effect of developing mass transfer boundary layers. The discrepancy at the lowest velocities was probably caused by natural convection and CO_2 gas bubbling.

As a more general case, equivalent velocities for the pipe and the cylinder can be calculated which guarantee identical mass transfer conditions[10,11] by selecting equations (5) and (6)

$$v_c = 0{\cdot}1066(\rho/\mu)^{0{\cdot}266}D^{0{\cdot}0371}(d_c^{0{\cdot}429}/d_p^{0{\cdot}2})v_p^{1{\cdot}229} \quad . \quad . \quad (7)$$

This equation, as well as the mass transfer measurements, enabled selection of the velocity in the SP and the corresponding rotating speed for the RC that would give identical mass transfer rates for the two geometries. It was found that, by selecting $v_p = v_c = 2\ m\ s^{-1}$, practically identical mass transfer coefficients of $(k_m)_p = (k_m)_c \sim 4 \times 10^{-4}$ $m\ s^{-1}$ at 20°C were measured. This is approximately in the middle of the region where the two curves overlap (Fig. 6). The majority of the corrosion experiments discussed below were conducted with $v_p = v_c = 2\ m\ s^{-1}$ (3820 rev min^{-1}), at which the mass transfer conditions were approximately equal.

CO_2 corrosion

Corrosion experiments without inhibitors

The corrosion experiments were carried out at room temperature (20–22°C) at pH 4, 5, and 6. The velocity was varied from stagnant to 13 $m\ s^{-1}$. Experiments were started by measuring the polarisation resistance (corrosion rate) every 30 min, at $v_p = v_c = 2\ m\ s^{-1}$ (equivalent mass transfer conditions). Typically, 24 h after the beginning of the experiments, measurements of the polarisation resistance (corrosion rate) and the corrosion potential as a function of the velocity were made. The velocity was varied from zero to 13 $m\ s^{-1}$ and back in the SP section and from zero

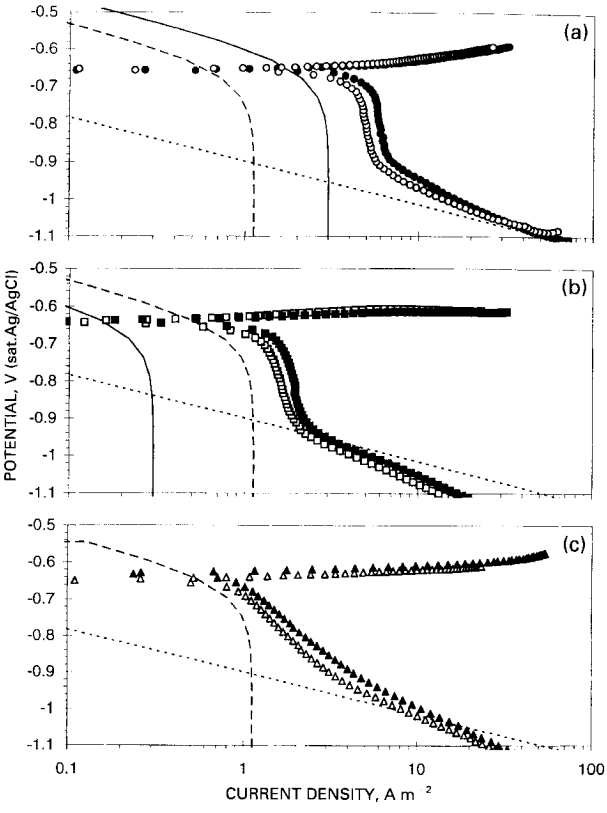

open symbols pipe flow; filled symbols rotating cylinder; —— H^+; --- H_2CO_3; · · · H_2O
a pH 4; *b* pH 5; *c* pH 6

7 *Potentiodynamic sweeps for given pH values conducted at $T = 20°C$ and equivalent mass transfer conditions: $v_p = v_c = 2\ m\ s^{-1}$ (3820 rev min^{-1}), 1%NaCl solution, $p_{CO_2} = p_{total} = 1$ bar, $d_c = 0{\cdot}01$ m, $d_p = 0{\cdot}015$ m*

to 5000 rev min^{-1} and back in the RC chamber. All this was completed within 2–5 h. Subsequently, the velocity was adjusted back to $v_p = v_c = 2\ m\ s^{-1}$. After a waiting period of 12 h (to obtain stable corrosion rates), electrochemical impedance measurements were conducted. Finally, potentiodynamic sweeps were obtained and the specimens were taken out from the loop and prepared for SEM analysis.

The potentiodynamic sweeps measured at $v_p = v_c = 2\ m\ s^{-1}$ (equivalent mass transfer conditions) and different pH are shown in Fig. 7. The measured curves are overlaid with theoretical curves predicted using the model of Nesic *et al.*[12] for easier interpretation of the corrosion mechanisms. The data obtained for the RC electrode are in good agreement with the data from the SP section over the entire potential range for all three pH values. According to the model, Fig. 7 shows the large contribution of the H^+ reduction reaction at pH 4 which is diminished at pH 5 and completely disappears from the figure at pH 6. At pH 5 and 6, the dominant cathodic reaction at the corrosion potential is direct H_2CO_3 reduction and, for more negative overpotentials, H_2O reduction. Good agreement between the RC and SP measurements is clear for all three cathodic reactions as well as for the anodic reaction. This leads to the conclusion that the same mechanism of CO_2 corrosion operated in the two flow geometries (RC and SP) at 20°C.

The potentiodynamic sweeps shown in Fig. 7 have been corrected for the solution resistance found by the electrochemical impedance technique. Figure 8 shows results of the electrochemical impedance measurements (Nyquist plots) at 20°C, pH 6, and $v_p = v_c = 2\ m\ s^{-1}$. Good agreement between the measured polarisation resistance values for the RC and SP geometries is shown. When the difference between specimen geometry areas is taken into account

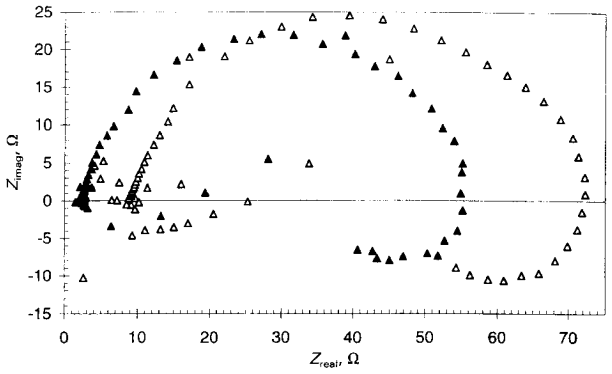

△ pipe flow; ▲ rotating cylinder

8 *Electrochemical impedance measurement at $T = 20°C$, 1%NaCl solution, pH 6, $p_{CO_2} = p_{total} = 1$ bar and equivalent mass transfer conditions: $v_p = v_c = 2$ m s^{-1} (3820 rev min^{-1}), $d_c = 0{\cdot}01$ m, $d_p = 0{\cdot}015$ m*

(10% larger for the RC), the measured polarisation resistances for the two geometries are even closer. The similar shapes of the measured curves confirm that an identical mechanism of CO_2 corrosion occurred in both flow geometries.

The corrosion rates obtained are shown as a function of velocity at 20°C in Fig. 9 for the different pH values. Corrosion is expressed as current and the corresponding corrosion rate (for iron dissolution, the relation 1 mm/year = 1·155 A m^{-2} was used). In Fig. 9, the results have been corrected for the presence of traces of oxygen by subtracting the contribution of the oxygen reduction current. Measured oxygen concentration varied from 10

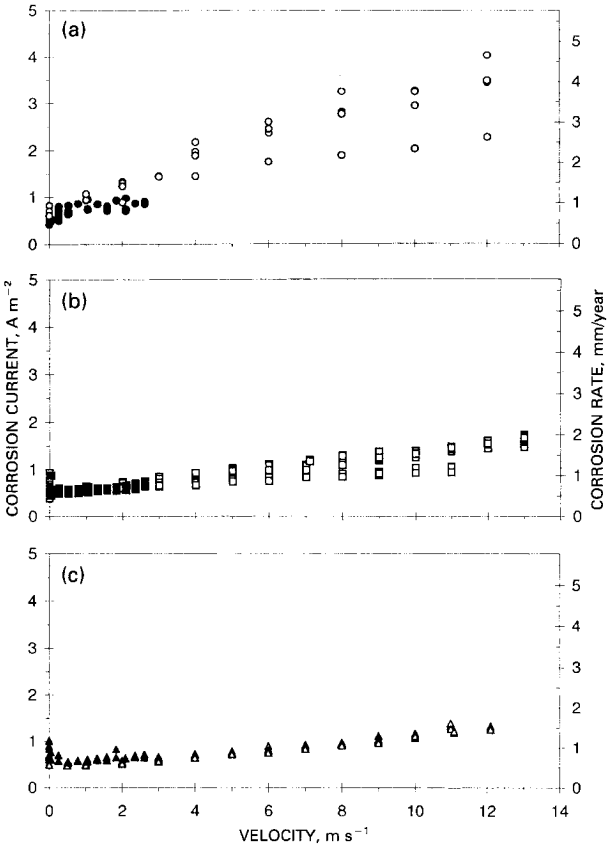

open symbols pipe flow; filled symbols rotating cylinder
a pH 4; *b* pH 5; *c* pH 6

9 *Effect of velocity on corrosion rate at given pH values at $T = 20°C$, 1%NaCl solution, $p_{CO_2} = p_{total} = 1$ bar, $d_c = 0{\cdot}01$ m, $d_p = 0{\cdot}015$ m*

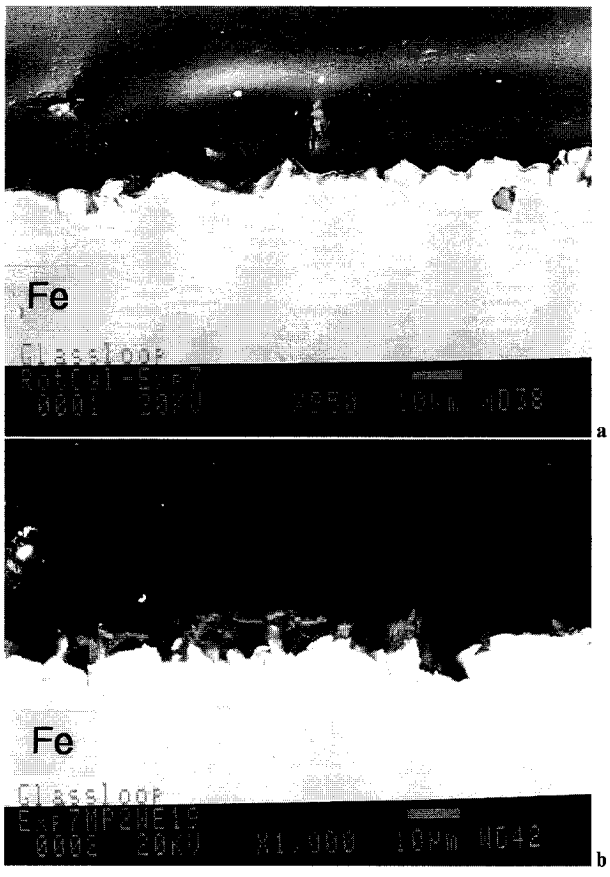

a rotating cylinder specimen; *b* straight pipe specimen

10 *Scanning electron microscope images of cross-sections of corroded surfaces exposed for 63 h to 1%NaCl solution at $T = 20°C$, pH 5, $p_{CO_2} = p_{total} = 1$ bar and equivalent mass transfer conditions: $v_p = v_c = 2$ m s^{-1} (3820 rev min^{-1}), $d_c = 0{\cdot}01$ m, $d_p = 0{\cdot}015$ m*

to 40 ppb in different experiments. To calculate the oxygen reduction current, the mass transfer correlations in equations (5) and (6) for the limiting current were used along with the diffusion coefficient for oxygen $D_{O_2} = 2{\cdot}09 \times 10^{-9}$ m^2 s^{-1} at 20°C. The B value was calculated for each point using the model of Nesic *et al.*,[12] and varied typically between 16 and 22 mV.

The corrosion rates under stagnant conditions were approximately the same for all three pH values, as shown in Fig. 9. As the velocity increased, the limiting current for H^+ reduction increased, leading to an increased overall cathodic reaction and a higher corosion rate. The increase of the corrosion rate with velocity was most pronounced at pH 4, where the concentration of H^+ was highest. In Fig. 9, it can be further noted that good agreement was obtained for the corrosion rates of the RC and SP specimens. This suggests that, in the absence of surface films, identical corrosion rates can be obtained by setting equivalent water chemistry and mass transfer conditions in the two flow geometries. It also confirms that, in the present case, the understanding of the CO_2 corrosion mechanisms permits the transfer of data from one flow system to another.

Figure 10 shows SEM images of the cross-sections of specimens exposed for 63 h to 1%NaCl solution at 20°C and pH 5. An evenly attacked surface virtually free of any films can be observed in each case.

Corrosion experiments with inhibitors

Experiments were carried out in which measurements were simultaneously conducted in the SP and RC sections, to

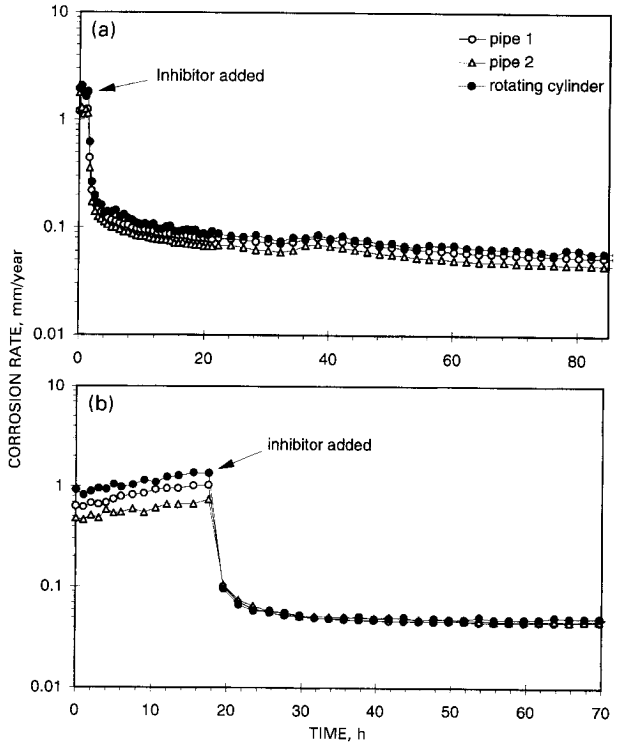

a 30 ppm ABI, 21°C; *b* 20 ppm IBI, 20°C

11 *Comparison of effects of given inhibitor on corrosion rate for straight pipe specimen at 2 m s^{-1} and rotating cylinder specimen at 3830 rev min^{-1}; pH 4, 1%NaCl solution, $p_{CO_2} = p_{total} = 1$ bar, $d_c = 0{\cdot}01$ m, $d_p = 0{\cdot}015$ m*

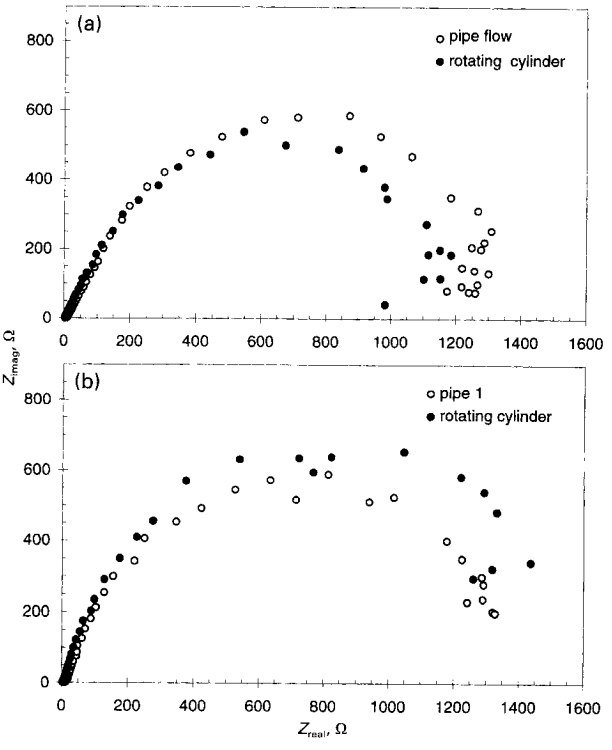

a 30 ppm ABI, 21°C; *b* 20 ppm IBI, 20°C

13 *Comparison of electrochemical impedance measurements obtained for straight pipe specimen at 2 m s^{-1} and rotating cylinder specimen at 3830 rev min^{-1} in presence of given inhibitor: 1%NaCl solution, pH 4, $p_{CO_2} = p_{total} = 1$ bar, $d_c = 0{\cdot}01$ m, $d_p = 0{\cdot}015$ m*

check whether a bench size apparatus (e.g. glass cell with a rotating cylinder) could be successfully used for the testing of corrosion inhibitors. The velocity in the SP test section

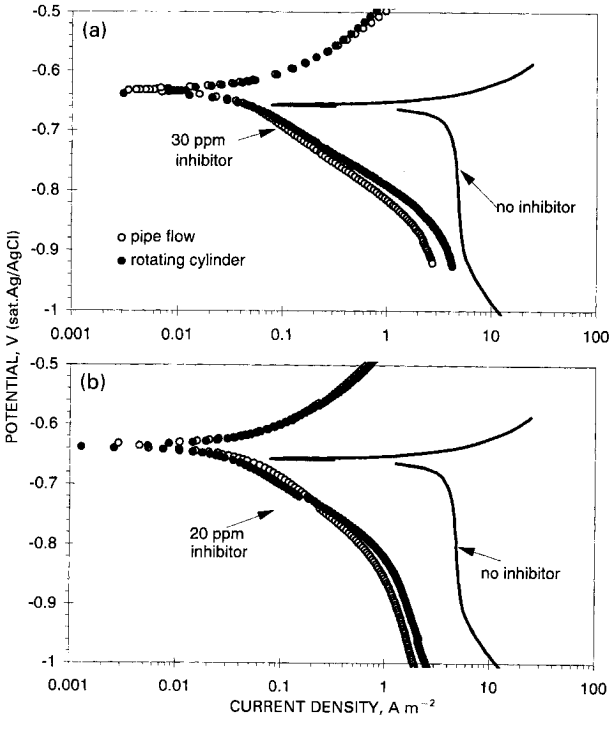

a ABI; *b* IBI

12 *Potentiodynamic sweeps obtained for straight pipe specimen at 2 m s^{-1} and rotating cylinder specimen at 3830 rev min^{-1} with and without presence of given inhibitor: 1%NaCl solution, pH 4, $T = 20$°C, $p_{CO_2} = p_{total} = 1$ bar, $d_c = 0{\cdot}01$ m, $d_p = 0{\cdot}015$ m; scan rate 0·2 mV s^{-1}*

was maintained at $v_p = 2$ m s^{-1} while the RC electrode was rotating at 3820 rev min^{-1} ($v_c = 2$ m s^{-1}). As demonstrated above, this guarantees the same mass transfer conditions and similar shear stresses in the two test sections. After addition of the inhibitor, the corrosion rate was reduced in both the RC and SP test sections to a low value for both inhibitors (Fig. 11). The kinetics of reduction of the corrosion rate were identical, as were the steady state corrosion rates. This suggests that the mechanism of protection was identical in both flow geometries. This finding was confirmed by considering the potentiodynamic sweep measurements (Fig. 12) and the electrochemical impedance measurements (Fig. 13). A similar conclusion was reached by Chesnut and Choi,[13] who found good agreement between rotating cylinder and straight pipe flows when testing inhibitors at the same shear stress. However, many other studies reached the opposite conclusion. It is believed by the present authors that, in most of those cases, the discrepancy arose from differing hydrodynamic and mass transfer conditions or, most probably, differing water chemistries in the two flow systems. As pointed out above, in the present study, even small traces of 'contamination' in the experimental apparatus are sometimes sufficient to radically change the performance of certain inhibitors. Surface films (corrosion products or scales) can have a similar effect.

It has repeatedly been assumed that high velocities (shear stresses) can be responsible for the failure of certain inhibitors to protect the metal surface from corrosion. The effect of extreme flow conditions on CO_2 corrosion in the presence of inhibitors was studied in the present case by varying the velocity from 2 to 10 m s^{-1}, corresponding to shear stresses of 13 and 222 Pa respectively. Results are shown in Fig. 14*a* for an experiment conducted with 30 ppm of ABI at pH 4, $T = 21$°C, and $p_{CO_2} = 1$ bar. When the velocity was varied from 2 to 10 m s^{-1} and back, only a small change in the corrosion rate was obtained. The

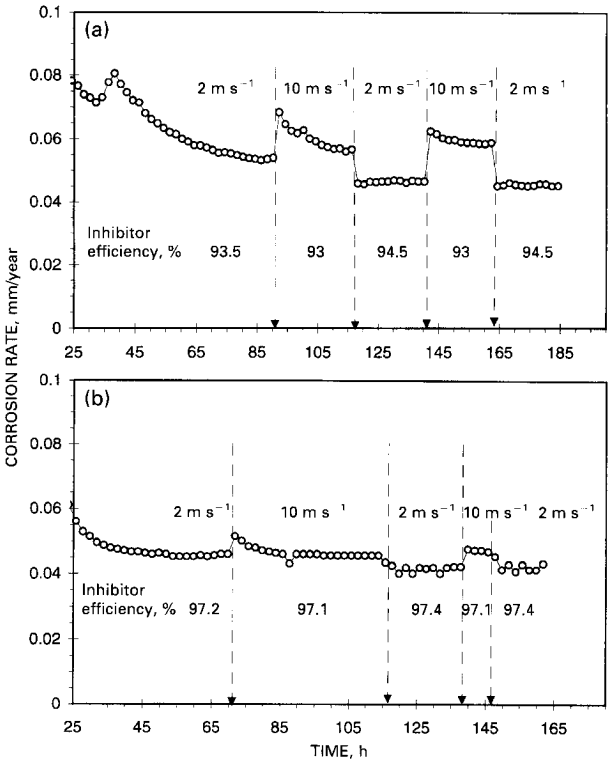

a 30 ppm ABI, 21°C; *b* 20 ppm IBI, 20°C

14 *Effect of pipe flow velocity on corrosion rate in presence of given inhibitor: 1%NaCl solution, pH 4,* $p_{CO_2} = p_{total} = 1$ *bar,* $d_p = 0{\cdot}015$ *m*

variation can be explained by an increased rate of mass transfer of H^+ ions (cathodic reactants). However, it can be concluded that the performance of the ABI inhibitor was not significantly affected by the flow, as the observed variations are within the margin of experimental error. Similar behaviour was found for the IBI inhibitor as shown in Fig. 14*b*. This conclusion can not be generalised as it is possible that different inhibitors may exhibit very different behaviours under extreme flow conditions.[3,13,14]

CONCLUSIONS

1. In the case of CO_2 corrosion in the absence of inhibitors:

(i) good agreement was obtained between the measured mass transfer coefficients and those predicted using the correlation of Berger and Hau for straight pipe flow and the correlation of Eisenberg *et al.* for the rotating cylinder flow geometry. This enabled selection of a velocity in the pipe and a corresponding speed for the rotating cylinder that gave approximately equal mass transfer conditions for the two geometries

(ii) it is possible to achieve the same mechanism and obtain approximately the same rate of CO_2 corrosion at a rotating cylinder and a straight pipe electrode by setting identical water chemistry and mass transfer conditions for the two flow geometries.

2. When inhibitors were added:

(i) the performances of both the ABI and IBI measured using the rotating cylinder were identical to those in the straight pipe flow geometry

(ii) the performance of the inhibitors was not significantly affected by flowrate in the range from 2 to 10 m s^{-1} (corresponding to shear stresses of 13 and 222 Pa respectively).

REFERENCES

1. K. D. EFIRD: *Corrosion*, 1977, **33**, 3.
2. S. NESIC and J. POSTLETHWAITE: *Corrosion*, 1990, **46**, 874.
3. J. L. DAWSON, C. C. SHIH, R. G. MILLER, and J. W. PALMER: Proc. Conf. Corrosion 90, Las Vegas, NV, USA, April 1990, NACE, Paper 14.
4. K. D. EFIRD, E. J. WRIGHT, J. A. BOROS, and T. G. HAILEY: Proc. Conf. Corrosion 93, New Orleans, LA, USA, March 1993, NACE, Paper 91.
5. 'Perry's chemical engineers' handbook', 7th edn, 6.10; 1997, New York, NY, McGraw-Hill.
6. D. R. GABE and F. C. WALSH: *Appl. Electrochem.*, 1983, **13**, 3.
7. F. P. BERGER and K.-F. F.-L HAU: *Int. J. Heat Mass Transfer*, 1977, **20**, 1185.
8. M. EISENBERG, C. W. TOBIAS, and C. R. WILKE: *J. Electrochem. Soc.*, 1954, **101**, 306.
9. P. W. ATKINS: 'Physical chemistry', 2nd edn, 905; 1982, Oxford, Oxford University Press.
10. V. E. HEITZ: *Werkst. Korros.*, 1964, 63.
11. T. CHEN. A. A. MOCCARI, and D. D. MACDONALD: Proc. Conf. Corrosion 91, Cincinatti, OH, USA, March 1991, NACE, Paper 292.
12. S. NESIC, J. POSTLETHWAITE, and S. OLSEN: Proc. Conf. Corrosion 95, Orlando, FL, USA, March 1995, NACE, Paper 131.
13. G. CHESNUT and H. J. CHOI: Proc. Conf. Corrosion 94, Baltimore, MD, USA, February–March 1994, NACE, Paper 35.
14. G. SCHMITT, T. SIMON, and R. H. HAUSLER: Proc. Conf. Corrosion 90, Las Vegas, NV, USA, April 1990, NACE, Paper 22.